

Ni-induced giant stress and surface relaxation in W(110)H. L. Meyerheim,* D. Sander, R. Popescu, and J. Kirschner
*Max-Planck-Institut für Mikrostrukturphysik, Weinberg 2, D-06120 Halle, Germany*O. Robach and S. Ferrer
*European Synchrotron Radiation Facility, B.P. 220, F-38043 Grenoble, France*P. Steadman
Department of Physics and Astronomy, E.C. Stoner Laboratory, University of Leeds, Leeds LS2 9JT, United Kingdom
(Received 4 March 2003; published 30 April 2003)

Atomic structure and surface stress changes are measured simultaneously by surface x-ray diffraction and by the crystal curvature technique during the deposition of Ni on W(110). Substantial lateral shifts of up to 0.5 Å of the W atoms upon deposition of the first layer Ni are detected. This unexpected restructuring of the W surface is correlated with compressive surface stress of $\tau_{1\bar{1}0} = -1$ N/m and $\tau_{001} = -2.1$ N/m. The atomic coordinates for Ni and W atoms of this c -(1×7) structure are given and they indicate the formation of chains between Ni and W atoms along $W[1\bar{1}1]$.

DOI: 10.1103/PhysRevB.67.155422

PACS number(s): 68.35.Ct, 61.10.-i

Surface stress has been recognized a decisive factor which determines a variety of phenomena like self-assembled pattern formation on the nanoscale, shape evolution of nano-objects and surface reconstruction.¹ In contrast to the important role of surface stress in the discussion of these effects, a general understanding of the relevant principles which govern the evolution of stress in the surface region of clean and adsorbate-covered solids is still lacking.² Especially the role of lattice misfit between adsorbate and substrate for the resulting stress remains intriguing. For some systems, the misfit-induced stress is reasonably well described by continuum elasticity,³ whereas for Fe/W(110) and Ni/W(110), misfit does not even give a qualitatively correct description of stress in the surface layer: compressive stress is measured where lattice misfit suggests tensile stress.⁴

Our present work reveals an important aspect of adsorbate-induced stress which might be of key importance for a general understanding of stress-strain relations in the monolayer range. We identify an intimate correlation between structure and stress from an in situ combination of surface x-ray diffraction (SXR) and stress measurements. Our structural investigation reveals substantial adsorbate-induced relaxation of substrate atoms in a system, which is generally regarded as structurally inert, and where structural relaxation has been neglected so far. We suggest that the failure of stress-strain relations is partially due to the inappropriate structural data of former investigations, where a bulklike substrate structure was tacitly assumed. However, here we present clear evidence for a Ni-induced reconstruction of the W(110) surface upon completion of the first Ni layer. This reconstruction is new, to our knowledge, as no adsorbate-induced reconstruction of W(110) has been confirmed so far.⁵ It is unexpected, as adsorption of the chemically similar element Fe did not induce a lateral distortion of the W(110) surface.⁶

We report in this paper on simultaneous SXR and stress measurements during growth of one layer Ni on W(110). We show that one atomic layer of Ni induces substantial lateral

shifts of the top layer W atoms of up to 0.5 Å. At this coverage we measure an anisotropic change of surface stress induced by Ni of $\tau_{1\bar{1}0} = -1$ N/m and $\tau_{001} = -2.1$ N/m.

The experiments were carried out at the beamline ID-3 of the European Synchrotron Radiation Facility (ESRF) in Grenoble using a six circle ultrahigh-vacuum diffractometer operated in the z -axis mode.⁷ For the SXR and stress measurements the W(110) crystal with dimensions $12 \times 2 \times 0.1$ mm³ was clamped at one end to a manipulator to allow free two-dimensional bending.³ The sample was cleaned by cycles of heating to 1500 K in 10^{-6} -mbar O₂ and subsequent annealing to 2400 K until no traces of impurity could be detected by Auger electron spectroscopy Ni was evaporated from a high purity Ni rod onto the substrate with a rate of approximately 200 s per layer at a substrate temperature of 300 K. During Ni deposition, the crystal curvature and the intensity of a selected x-ray diffraction peak were measured simultaneously. The crystal curvature was monitored during Ni deposition by reflecting a laser beam from the W substrate onto a position sensitive detector. Thus, stress-induced changes of the crystal curvature lead to a deflection of the reflected laser beam, which is detected by the respective change of the position signal. Biaxial stress is calculated from the measured curvature along $W[001]$ and $W[1\bar{1}0]$.⁸ Thus, the formation of a certain surface structure is unequivocally correlated with the respective stress state.

From earlier experiments it is known that Ni grows in the Nishiyama-Wassermann orientation on W(110), which leads to the formation of additional, so-called satellite diffraction spots along $W[001]$, whereas no change of periodicity was observed along $W[110]$, and a c -(1×7) diffraction image is observed by low energy electron diffraction.⁹

The biaxial Ni-induced stress change of the W(110) surface is presented in Fig. 1(a), and Fig. 1(b) displays the corresponding intensity of a satellite reflection characteristic for the c -(1×7) superstructure. The intensity due to a strong satellite reflection (1 9 0.2) (Ref. 10) remains zero up to the

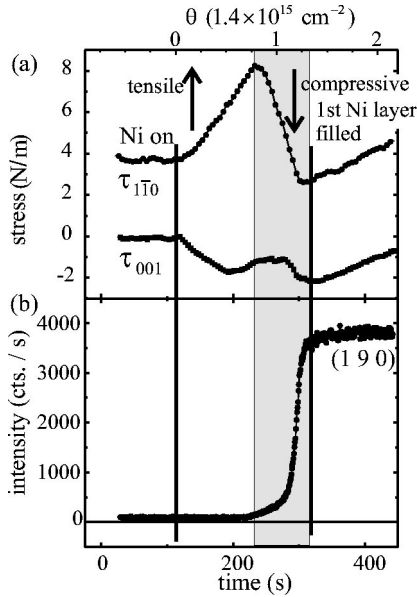


FIG. 1. (a) Biaxial stress along $W[1\bar{1}0]$ and $[001]$ vs Ni-deposition. ($\theta=1:1.41\times 10^{15}$ atoms/cm²). The upper stress curve is shifted vertically for clarity. (b) Intensity of a SXRDR reflection characteristic for the 1×7 superstructure versus deposition time. The formation of the 1×7 superstructure coincides with compressive stress along both directions. The shaded region indicates the coverage where the formation of the c -(1×7) evolves. The thick vertical line at $\theta=1.3$ indicates the coverage of the structural investigation presented in Figs. 2 and 3.

deposition of $\theta=0.8$ ($\theta=1:1.41\times 10^{15}$ atoms/cm²). In this coverage regime, the stress curves indicate compressive stress along $[001]$, and tensile stress along $[110]$. This anisotropy of the Ni-induced stress is ascribed to the change of the surface stress of W upon Ni adsorption. In short, the stress change is qualitatively comparable to the system Fe on W(110) up to $\theta=0.5$, where the stress anisotropy has been ascribed to the topology of the bonds of W(110).⁴ In the following, we concentrate on the filling of the W surface at a Ni coverage of $\theta=1.3$.

The intensity of the $(1\ 9\ 0.2)$ reflection develops for $\theta>0.8$, and the emergence of the c -(1×7) superstructure intensity coincides with the formation of compressive stress. This coverage regime is emphasized by the shaded area in Fig. 1. The stress changes most prominently along $W[110]$, where a change from tensile to compressive stress is measured. At the completion of the first Ni layer at $\theta=1.3$, a compressive stress of $\tau_{1\bar{1}0}=-1$ N/m and $\tau_{001}=-2.1$ N/m results. The change of sign of stress along $[110]$ with increasing Ni coverage is unexpected, as no change of the packing density of Ni atoms along $W[110]$ can be inferred from the c -(1×7) structure.⁸ This is in contrast to the higher packing density along $[001]$ upon formation of the c -(1×7) structure, which offers a plausible explanation for the compressive stress along $[001]$. The following structural analysis of this first Ni layer at $\theta=1.3$ identifies substantial lateral shifts of both W and Ni atoms away from what one might have expected to be ideal c -(1×7) bonding sites.

The structure factor amplitudes $|F_{hkl}|$ were derived from

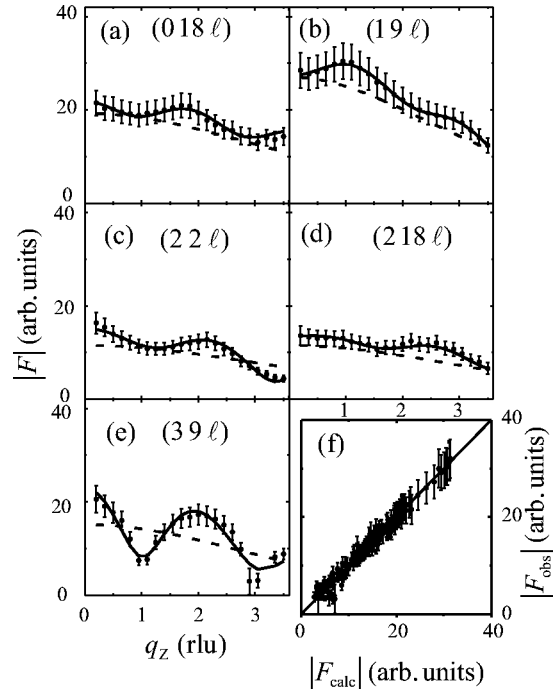


FIG. 2. (a)–(e) Measured (symbols) and fitted (lines) structure factor amplitudes along several superlattice rods. The solid lines correspond to the best fit. The dashed lines represent a simplistic model where the W substrate positions are fixed to the bulk values. The indices of the rods are related to the 1×7 setting of the unit cell. (f): Plot of $|F_{\text{calc}}|$ vs $|F_{\text{obs}}|$ for all data. The data are closely aligned along the diagonal corresponding to the $|F_{\text{calc}}|=|F_{\text{obs}}|$ condition indicating a high quality fit.

the integrated intensities after correcting the data for active sample area, polarization, and Lorentz-factor.¹¹ Figures 2(a)–2(e) shows as solid symbols the $|F_{hkl}|$ along five superlattice rods measured up to a maximum normal momentum transfer of $l=q_z/c^*=3.5$ reciprocal lattice units (rlu, with $c^*=0.223\ \text{\AA}^{-1}$) in steps of $\Delta l=0.15$ rlu using a detector resolution of 0.02 rlu. Figure 2(f) plots all 144 experimental structure factors (35 of them measured at $l=0.2$ rlu) vs the calculated structure factors as derived from a structural model, which is discussed below. All $|F|$ values are closely aligned along the diagonal in Fig. 2(f), which represents the ideal condition $|F_{\text{obs}}|=|F_{\text{calc}}|$. The small scatter of the data points from the diagonal and the good description of the experimental data points by the calculated $|F|$'s shown as solid lines in Figs. 2(a)–2(e) indicate the validity of the structural model. Quantitatively this is expressed by the small unweighted residual (R_u) of 0.05.¹² The statistical more relevant goodness-of-fit parameter, which takes the number of refined parameters (25) and the number of reflections (144) into account, was in the 1.0 regime. This indicates a well satisfying fit with all reflections fitted with an accuracy of about one standard deviation as is also evident by inspection of Fig. 2. The broken line in Figs. 2(a)–2(e) indicates calculated $|F|$ for a simplistic structure model, as described below.

A visual inspection of Figs. 2(a)–2(e) reveals a non-

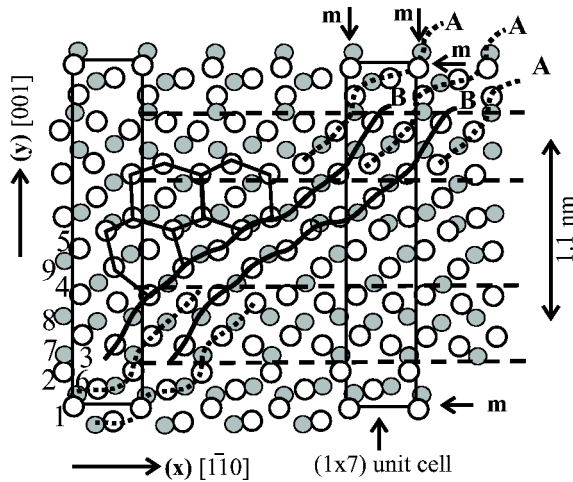


FIG. 3. Model of the Ni/W(110) superstructure in top view. Bright and dark circles correspond to Ni and W atoms, respectively. The rectangle indicates a 1×7 unit cell (size: $22.16 \times 4.47 \text{ \AA}^2$). Two inequivalent Ni-W-Ni chains are labeled (A) and (B). The numbers identify the atoms as in Table I.

monotonic variation of the structure factor amplitudes with q_z , which is qualitatively described by a modulation periodicity $\Delta l = 2 \text{ rlu}$. This directly indicates, that two layers at an approximate distance of $c/2$ (2.2 \AA) contribute to the diffraction at non-Bragg positions. We have shown in a previous scanning tunneling microscopy study that at this Ni coverage of 1.3 all Ni atoms are bonded in the first Ni layer on top of the W substrate.¹³ From this we deduce that the modulation is related to the interference between the top layer (Ni) and the second layer (W). A distortion of a single layer (even with maximum corrugation in the order of 0.5 \AA) would only give rise to a slow monotonic decrease of the intensities along q_z , as shown by the broken lines in Figs. 2(a)–2(e). We conclude that both top Ni layer and first W layer are driven in a c - (1×7) structure.

A quantitative structure analysis was carried out by least square fitting of the $|F|^2$'s to a structure model. A top view of the best fit model ($R_w = 0.05$) is presented in Fig. 3. Several 1×7 unit cells (two are indicated by the solid rectangles) are plotted to clarify the structural characteristics. The Ni and W atoms are represented as bright and dark circles, respectively.

The Ni surface structure on W(110) can be described as a densely packed distorted hexagonal network. This is emphasized in Fig. 3 by some hexagons with Ni atoms at the edges and one in the center. A more detailed view reveals that the most prominent feature of the structure are alternating Ni-W-Ni chains along $[1\bar{1}1]$. They are labeled A and B, respectively. The chains (approximate length: 25 \AA) are composed of nine Ni atoms and seven W atoms, where the Ni atoms are located at or close to bridge sites between the W atoms. Several A- and B-type chains are emphasized by solid and dashed lines, respectively. It can be seen, that while chains A and B are neighbored by chains of the same type over most of their length (A-A or B-B), there is some overlap regime ($\approx 5 \text{ \AA}$), where A and B are neighbored by B and A respectively. These regions are indicated in Fig. 3 by the dashed lines running parallel to $[1\bar{1}0]$. The overlap regions are sepa-

TABLE I. Coordinates (x, y, z) of Ni and W atoms within the asymmetric unit of the (1×7) unit cell ($cmm2$ plane group) in relative units of the unit cell dimensions as given in Ref. 9. The numbers of the atoms refer to the labels in Fig. 3 “ \pm ” indicates a half-occupied split position off the mirror line running along $x = 0.0$ or $y = 0.0$, respectively. The coordinates in brackets indicate the y positions for a model with equally spaced Ni atoms along $[001]$ and y positions of bulk truncated W, respectively. Error bars are of the order of ± 0.02 lattice units, and the z coordinates of W are fixed.

	x	y	z
Ni(1)	± 0.015	± 0.005 (0.0)	0.46
Ni(2)	± 0.108	0.110 (1/9)	0.48
Ni(3)	± 0.170	0.202 (2/9)	0.52
Ni(4)	± 0.131	0.324 (3/9)	0.51
Ni(5)	± 0.118	0.455 (4/9)	0.41
W(6)	± 0.089	± 0.031 (0.0)	0.00
W(7)	± 0.097	0.145 (1/7)	0.00
W(8)	± 0.126	0.260 (2/7)	0.00
W(9)	± 0.138	0.441 (3/7)	0.00

rated by 1.1 nm along $[001]$, which corresponds to half the superlattice spacing along $[001]$. This structural detail is directly related to the scanning tunneling microscopy (STM) images of the c - (1×7) Ni structure, which show bright lines along $[1\bar{1}0]$, separated along $[001]$.⁸ Our model reveals that within the overlap-region the average height of the Ni-atoms above the W surface is about 0.3 \AA higher than in the remaining structure ($\approx 2.3 \text{ \AA}$ vs $\approx 2.0 \text{ \AA}$). This vertical corrugation together with the higher atom density of the overlap region offers a natural explanation of the STM contrast.⁸ Table I lists the atomic positions of the Ni and W atoms, as determined from the fit, for the asymmetric unit of the unit cell ($cmm2$ plane group).

The most important and astonishing aspect of this structure is the pronounced shift (up to 0.5 \AA) of the first-layer W atoms out of their bulk positions along $[1\bar{1}0]$. The inclusion of W distortions in deeper layers did not improve the fit quality, and such distortions were not considered. Our model also includes some W top-layer rumpling, which we consider by a Debye parameter of the order of $B = 5 \text{ \AA}^2$ (corresponding to a root mean square displacement of 0.25 \AA). Pronounced lateral disorder along $[1\bar{1}0]$ is also observed for the Ni atoms. For both Ni and W atoms the disorder is taken into account by introducing half occupied “split-positions” off the mirror lines running along $x = 0$ and $y = 0$ within the unit cell. Some mirror lines are indicated by the arrows in Fig. 3 and labeled by “m.” A split position at $\pm x$ or $\pm y$ means, that for the W and Ni atoms there is a 50% probability to occupy one of the two possible positions. Locally, in one of the four domains, the $cmm2$ plane group symmetry is destroyed (the symmetry of the domain is $p1$ only), however on average the $cmm2$ symmetry is preserved as observed by low energy electron diffraction and SXRD.¹⁴

We tested different structural models, such as more simplistic ones, which neglect the lateral disorder of the Ni and

W positions (i.e., without introducing split positions). However, these models yield significantly worse fits as characterized by agreement parameters larger by a factor of up to five. A calculation based on a bad model is shown by the broken lines in Figs. 2(a)–2(e). It gives a bad fit, as here only a single Ni-layer is considered in the structural analysis, whereas the appropriate analysis considers distortions of both the Ni and W layers. Based on the shortcomings of the worse models we are confident that our structural model presented in Table I is of significant physical relevance.

Our structural model leads to plausible inter-atomic distances for W and Ni atoms, which correspond within several percent to the bulk values of 2.74 and 2.49 Å, respectively. The average Ni-W distance is 2.6 ± 0.3 Å, which closely resembles the sum of the Ni and W atomic radii (2.64 Å).¹⁵

Our results elucidate the relation between compressive stress and structure of the c -(1×7) structure. The negative slope of the stress curves of Fig. 1(a) around $\theta=1.1$ indicates that the formation of the c -(1×7) superstructure is directly related to a giant compressive stress of –116 and –33 GPa, along $W[1\bar{1}0]$ and $[001]$, respectively. The magnitude and sign of the stress are in stunning conflict with elasticity theory which predicts a stress of –0.16 and +9.3 GPa along $[110]$ and $[001]$, respectively, for the anisotropic strain of

$\varepsilon_{1\bar{1}0}=0.037$ and $\varepsilon_{001}=-0.013$, which characterizes the c -(1×7) structure.^{8,16}

It has been a common approach to neglect any substrate relaxations upon metal adsorption for such systems, where no surface reconstruction had been observed. Our results show that the underlying assumption of bulklike in-plane and vertical atomic positions at the interface is not justified in general. Adsorption of Ni atoms on W(110) in the monolayer coverage range induces massive shifts of the first layer W atoms. Therefore, the Ni-W composite has to be considered in all cases where surface stress is studied. To what extent these atomic distortions are responsible for the measured compressive stress remains to be investigated by state-of-the-art calculations and our data provide benchmark values for these.

In conclusion, we have measured a substantial adsorbate-induced structural relaxation in a system, which is generally considered to be structurally inert upon adsorption. Simultaneous structure and stress measurements identify a striking correlation between the onset of lateral shifts of atomic positions and compressive surface stress. The implications of adsorbate-induced substrate relaxation are profound as the resulting elastic interactions are an important driving force for self-assembled pattern formation on the nanoscale.

*Corresponding author. FAX: ++49-345-5511-223. Email address: hmeyerhm@mpi-halle.de

¹B. Croset, Y. Girad, G. Prévot, M. Sotto, Y. Garreau, R. Pinchaux, and M. Sauvage-Simkin, *Phys. Rev. Lett.* **88**, 056103 (2002); A. Li, F. Liu, and M. G. Lagally, *ibid.* **85**, 1922 (2000); C. E. Bach, M. Giesen, H. Ibach, and T. L. Einstein, *ibid.* **78**, 4225 (1997).

²H. Ibach, *Surf. Sci. Rep.* **29**, 193 (1997); **335**, 71 (1999); P. J. Feibelman, *Phys. Rev. B* **56**, 2175 (1997).

³D. Sander and H. Ibach, in *Physics of Covered Surfaces*, edited by H. P. Bonzel, Landolt-Börnstein, New Series, Group III, Vol. 42, Pt. a (Springer, Berlin, 2002), Chap. 4.4, p. 4.4-1.

⁴D. Sander, A. Enders, and J. Kirschner, *Europhys. Lett.* **45**, 208 (1999).

⁵Reconstruction was erroneously claimed in J. W. Chung, S. C. Ying, and P. Estrup, *Phys. Rev. Lett.* **56**, 749 (1986); no reconstruction was claimed by M. Arnold, G. Hupfauer, P. Bayer, L. Hammer, K. Heinz, B. Kohler, and M. Scheffler, *Surf. Sci.* **382**, 288 (1997).

⁶H. L. Meyerheim, D. Sander, R. Popescu, J. Kirschner, P. Steadman, and S. Ferrer, *Phys. Rev. B* **64**, 0454141 (2001).

⁷S. Ferrer and F. Comin, *Rev. Sci. Instrum.* **66**, 1674 (1994).

⁸

$$\tau_i^{\text{Ni}} = \frac{Y t_W^2}{6(1-\nu^2)} \left(\frac{1}{R_i} + \nu \frac{1}{R_j} \right),$$

with $i, j = [100][1\bar{1}0]$, see Refs. 3 and 4. Stress: τ_i ; Ni thickness: t_{Ni} ; W substrate thickness: t_W , Young modulus W: Y ; Poisson ratio W: ν ; radius of curvature: R_i .

⁹D. Sander, C. Schmidhals, A. Enders, and J. Kirschner, *Phys. Rev. B* **57**, 1406 (1998), and references therein.

¹⁰The reflection indices are referred to the rectangular 1×7 unit cell with $a=4.476$ Å, $b=22.155$ Å, $c=4.476$ Å, and reciprocal lattice units (rlu) $a^*=1.404$ Å⁻¹, $b^*=0.284$ Å⁻¹, and $c^*=1.404$ Å⁻¹.

¹¹E. Vlieg, *J. Appl. Crystallogr.* **30**, 532 (1997).

¹²The unweighted residuum is defined as $R_u = \sum_{hkl} |F_{hkl}^{\text{obs}}| - |F_{hkl}^{\text{calc}}| / \sum_{hkl} |F_{hkl}^{\text{obs}}|$, where $|F_{hkl}^{\text{obs}}|$ and $|F_{hkl}^{\text{calc}}|$ are observed and calculated structure factor amplitudes, respectively.

¹³C. Schmidhals, D. Sander, A. Enders, and J. Kirschner, *Surf. Sci.* **417**, 361 (1998).

¹⁴Since the symmetry in the domain is $p1$ only, in total there are four domains related by mirror symmetry in order to restore the average $mm2$ point symmetry of the structure. Our model with split positions assumes coherent averaging over these domains.

¹⁵L. Pauling, *The Nature of the Chemical Bond* (Cornell University Press, Ithaca, NY, 1960).

¹⁶D. Sander, *Rep. Prog. Phys.* **62**, 809 (1999).